Unsteady Aerodynamic Simulation of Offshore Wind Turbines with Wave-wind Interaction

Ping Cheng [*], Yong Ai, Decheng Wan[‡]

State Key Laboratory of Ocean Engineering, School of Naval Architecture, Ocean and Civil Engineering, Shanghai Jiao Tong University, Collaborative Innovation Center for Advanced Ship and Deep-Sea Exploration, Shanghai 200240, China

[*]Presenting author: xiakee@sjtu.edu.cn

[‡]Corresponding author: dcwan@sjtu.edu.cn

http://dcwan.sjtu.edu.cn

Abstract

The aerodynamic simulation of an NREL-5MW baseline wind turbine is conducted. The three-dimensional Reynolds Averaged Navier-Stokes equations (RANS) are solved, and the k-ω SST turbulence model is used. The in-house code naoe-FOAM-os-SJTU solver based on OpenFOAM and overset grid technique is employed. The wave-wind interaction is studied first. The interaction between wind flow and with wave surface reduces the wind speed below certain height, and a shear wind model is obtained and employed as the non-uniform inflow wind for the unsteady aerodynamic simulation of wind turbine. The aerodynamic simulations of the 5-MW baseline wind turbine under uniform or non-uniform inflow wind are conducted respectively. With shear inflow wind, when the lower-speed layer overlaps the rotating region of turbine blades, the aerodynamic forces on turbine rotor oscillate with 1/3 rotating period.

Keywords: aerodynamic simulation; offshore wind turbine (OWT); overset grid technique; naoe-FOAM-os-SJTU solver

Introduction

As a kind of renewable and sustainable energy source, wind energy shows great potential to solve the worldwide energy and environment crisis. With special and strong advantages over traditional onshore wind turbines, offshore wind turbines (OWT) become more attractive. Accurate aerodynamic prediction of wind turbine is one of the common challenges in design of offshore wind turbines.

Most of the early aerodynamic simulations are conducted with uniform wind condition, while the wind velocity is reduced when the air moves against the surface of water wave (Atcheson, 2016). And shear wind causes oscillations of the aerodynamic forces and power generated by a wind turbine. These oscillations of forces have 1/3 rotating period for a three-bladed wind turbine (Thiringer, 2001). This oscillation on power may effects the output power quality and the control system, and the oscillations of aerodynamic forces could cause additional fatigue damages on the structure. Several studies on this oscillation caused by shear wind have been conducted. Bayne (2000) researched the power oscillation due to turbine blades encountering different wind speed at different vertical positions, and stated that the minimum power occurred when any individual blade pointed directly downwards. Dolan (2006) also study the oscillation on torque and power of a three-bladed wind turbine caused by shear wind and tower shadow effects, similar conclusions were drawn as Bayne did, which stated that the torque and power generated by a three-bladed wind turbine exists oscillation with 3 times the rotational frequency, and the maximum value of oscillating torque and power was observed

when one blade was pointed directly upstream and the minimum value was noted while one blade was pointed directly downstream.

In this paper, the unsteady aerodynamic performance of the NREL-5MW Baseline wind turbine with shear inflow wind is investigated. The three-dimensional Reynolds Averaged Navier-Stokes equations are solved for the aerodynamic numerical simulation. The naoe-FOAM-os-SJTU solver, which is based on OpenFOAM and overset grid technology and developed for ship and ocean engineering problems, is employed. In this paper, the interaction between wave and wind is studied first to get a proper shear wind model for unsteady aerodynamic simulations with non-uniform inflow wind. And aerodynamic simulations in three different inflow wind conditions are conducted. From the simulation, the time series of the unsteady torque and thrust are obtained, together with the detailed information of the wake flow field to clarity the detailed flow filed information.

1 Numerical Method

1.1 Governing Equations

In the numerical simulations in this paper, the incompressible Reynolds-Average Navier-Stokes (RANS) equations are solved, which contain the continuity equations and the momentum equations:

$$\frac{\partial U_i}{\partial x_i} = 0 \tag{1}$$

$$\frac{\partial U_i}{\partial t} + \frac{\partial}{\partial x_j}\left(U_i U_j\right) = -\frac{1}{\rho}\frac{\partial P}{\partial x_i} + \frac{\partial}{\partial x_j}\left(\nu \frac{\partial U_i}{\partial x_j} - \overline{u_i' u_j'}\right) \tag{2}$$

In these equations, U_i is the averaged flow velocity component, while u_i' is the fluctuation part; ρ is the density of the fluid; p is the pressure; ν is the kinematic viscosity.

But the equations are not closed as they contain more variables than there are equations. In order to meet the closure requirement and solve the above equations, the two-equation turbulence model k-ω SST (Menter, 1994) is employed, and the turbulent kinetic energy k and the turbulent dissipation rate ω can be described as:

$$\frac{\partial}{\partial \mathrm{t}}(\rho k) + \frac{\partial}{\partial x_i}(\rho k \,\mathrm{u}_i) = \frac{\partial}{\partial x_j}(\Gamma_k \frac{\partial k}{\partial x_j}) + \mathrm{G}_k - Y_k + S_k \tag{3}$$

$$\frac{\partial}{\partial \mathrm{t}}(\rho \omega) + \frac{\partial}{\partial x_i}(\rho \omega \,\mathrm{u}_i) = \frac{\partial}{\partial x_j}(\Gamma_\omega \frac{\partial \omega}{\partial x_j}) + \mathrm{G}_\omega - Y_\omega + D_\omega + S_\omega \tag{4}$$

Where, Γ_k and Γ_ω are the effective diffusion coefficients for the turbulent kinetic energy k and the turbulent dissipation rate ω respectively, G_k and G_ω are turbulence generation terms for k and ω, Y_k and Y_ω are turbulent dissipation terms for k and ω, S_k and S_ω are the source term for k and ω, D_ω is the cross-diffusion term for ω.

1.2 Overset Grid Technique

Using overset grid technique, the separated overlapping grids for each part with independent motion are allowed, which makes powerful in simulation of large amplitude motion problems. And the connection among grids of each part is built by interpolation at appropriate cells or points using DCI (domain connectivity information) which is produced by SUGGAR++.

(Noack, R.W. 2005b. Carrica, et al. 2010b). There are four main steps when using DCI in the overset grid technique: The first step is to mark the hole cells which are located outside the simulation domain or of no interest, and exclude them from computation. As shown in Fig.1, in each overset grid, there exist series of cells around hole cells named fringe cells, and for each fringe cell there are several donor cells which provide information from the donor grids, so the second step is to seek for the donor grids of each fringe cell and provide information from the donor grids. The third step is to obtain the value of a variable ϕ of the fringe cell by interpolation using Eq.1 from the donor cells find in the second step.

$$\phi_I = \sum_{i=1}^{n} \omega_i \cdot \phi_i \qquad (5)$$

Where ϕ_I is the value of a variable ϕ of the fringe cell, ϕ_i is the value for the i^{th} donor cell, ω_i is the weight coefficient, which is dimensionless and follows the condition shown in Eq.2:

$$\sum_{i=1}^{n} \omega_i = 1 \qquad (6)$$

And the last step is to optimize the overlapping area and improve the accuracy of interpolation.

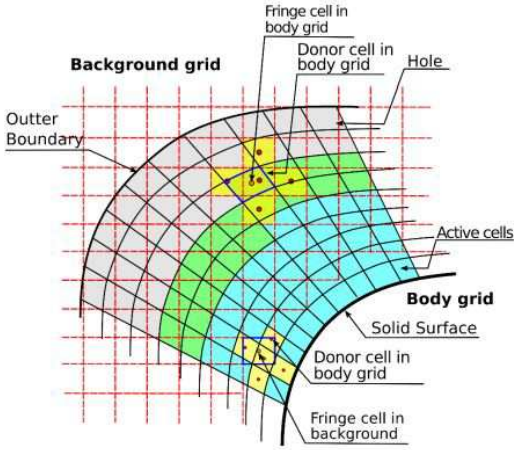

Fig. 1 Diagram of overset grid

2 Physical Model and Grid Structure

2.1 NREL-5MW Baseline Wind Turbine

The representative utility-scale NREL-5MW baseline wind turbine (Jonkman, 2009) is employed in current study. This is a three-bladed wind turbine and the length of each blade is 61.5m. For each blade, the cross sections from blade root to blade tip are composed of a series of DU_XXX and NACA64_XXX airfoils (Lindenburg, 2002). With these detailed data of blade and airfoils, the structural model is built (Bazilevs, 2011) which is shown in Fig.2.

Table 1. Summery of NREL-5MW Baseline Wind Turbine Properties

Rating Power	5MW
Rotor Orientation	Upwind
Rotor Diameter	126m
Hub Diameter	3m
Hub Height	90m
Maximum Rotor	12.1rpm
Maximum Tip Speed	80m/s
Overhang / Shaft Tilt / Precone	5m / 5º / 2.5º

Two overlapping meshes are generated to use the overset grid technique, which are the background mesh grid of the simulation domain generated, and the overlapping grids for the turbine rotor. Both the two set of grid are generated with OpenFOAM including the blockMesh and snappyHexMesh utilities.

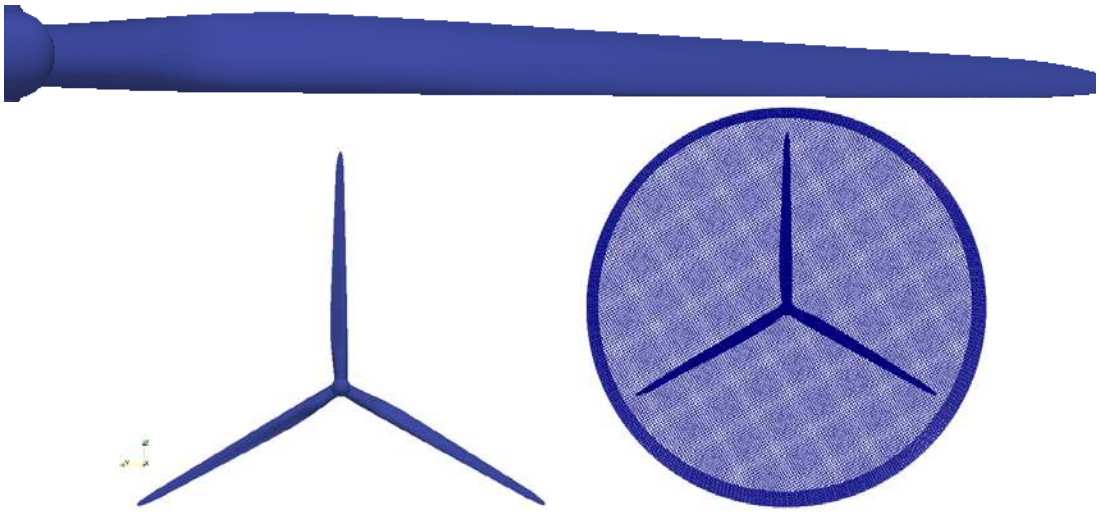

Figure 2. NREL-5MW Baseline Wind Turbine

In the turbine rotor grid system, a cylinder subdomain is built with radius of 72m, and width of 20m. and 3 levels of refinement around the blades are conducted using refineMesh utility in OpenFOAM, and another two levels of refinement are done before surface snapping, and six layers are set up at the surface grid. The total number of cells for this part of grid is about four million.

2.2 Setup of Simulation Domain

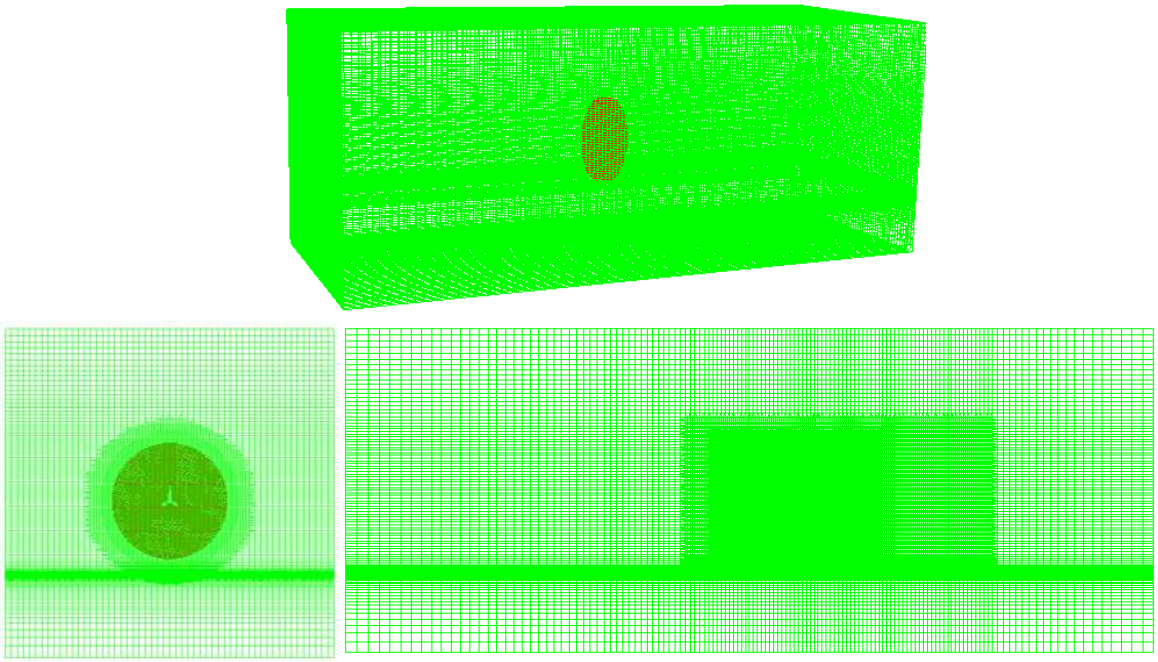

Figure 3. Setup of the simulation domain

According to the structural properties, the simulation domain is generated as a box (X: -500m~500m, Y: -200m~200m, Z: -100m~300m), which is shown in Fig.3. To improve the

simulation accuracy, refinement of the mesh around turbine blades is necessary, and proper mesh refinement in the wake flow field is also very important to capture the flow information in the wake flow. The region of refined mesh is a cylinder with radius of 110m, and length of 350m (-50m~300m). To take the wave-wind interaction into consideration, refinement of mesh near water free surface is also carried out. And the simulation of wave-wind interaction is conducted with this background grid system without refinement of the cylinder region.

3 Shear Wind Model

Most of the aerodynamic studies on the wind turbine are conducted in uniform inflow wind conditions. While with effects of free surface, the air velocity is reduced when moving against surface of wave. A wave-wind interaction study was conducted first to get the shear wind model. In the simulation domain described above, regular wave with period of 10s and wave length of 156m is generated, and the boundary condition of inlet is set as fixed inlet wind with wind speed distribution described as case2 in table.2. After 100s simulation, the steady state of the wave-wind interaction is available.

Fig.3 shows the distribution of wind velocity with increase of height from still water level (z=0) at x=0, where the center of turbine rotor locates. As the free surface changes all the time, which may cause the variation of the flow velocity, velocity distributions at four typical moments during one complete wave period (T0=200s, T0+1/4T, T0+2/4T, T0+3/4T) are presented in Fig.4. Comparing these four sets of data, tiny differences are observed, which mainly lie in lower areas where height is less than 40m. As introduced above about the NREL-5MW wind turbine, the rotational center of this turbine lies 90m above the still water level, and the diameter of rotor blade is 126m. So the lowest point of the rotating blade is above 27m (not equal to 27m because of the shaft tilt of the rotor plane and the precone of each blade introduced in Table.1). So the differences between velocity distributions at different moments during a wave period are negligible. With these data, a fitting curve is achieved as the red line in Fig.4. With wave-wind interaction, the wind speed in lower area decreased obviously, while the wind velocity in the above area gets increased.

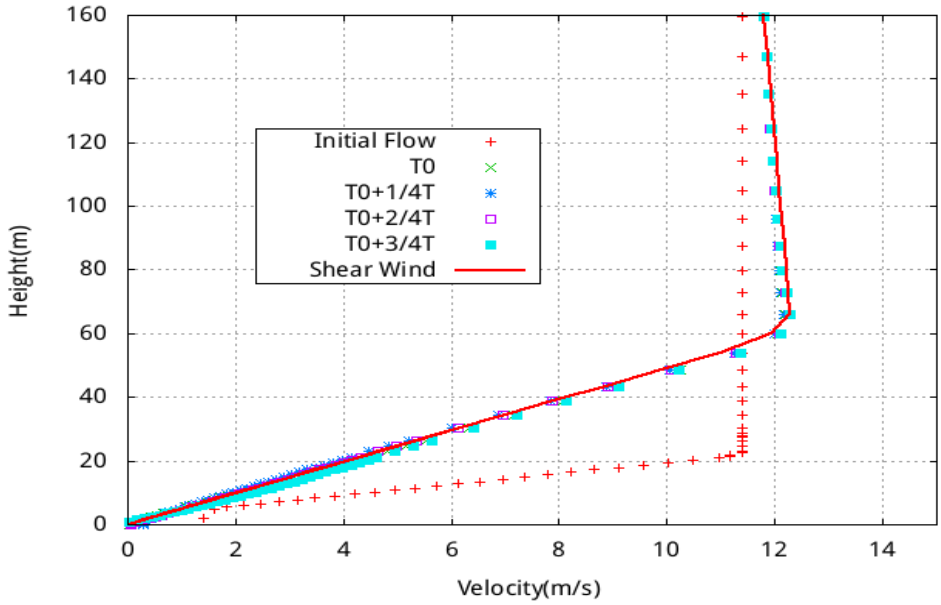

Figure 4. The shear wind model

In this paper, three simulation cases are conducted (Table.2). Uniform inflow wind with wind speed U=11.4m/s is for case1, linear type shear wind described as a piecewise function shown in table.2 is set in case2, and the fitting curve shown in Figure.3 is applied on inlet boundary as well as initialization of the flow field in case3. The initial wind velocity distributions in three cases are shown in Fig.5.

Table 2. Setup of simulation cases with different wind velocity distribution

No.	Cases	Description of inflow wind speed
1	Uniform Wind	U=11.4m/s
2	Linear Shear Wind	$U=\begin{cases}11.4*(20-z)/20 & z<20\\ 11.4 & z\geq 20\end{cases}$ (m/s)
3	Shear Wind with Wave-wind Interaction	Fitting curve ("shear wind") shown in Fig.4

(a) Uniform wind

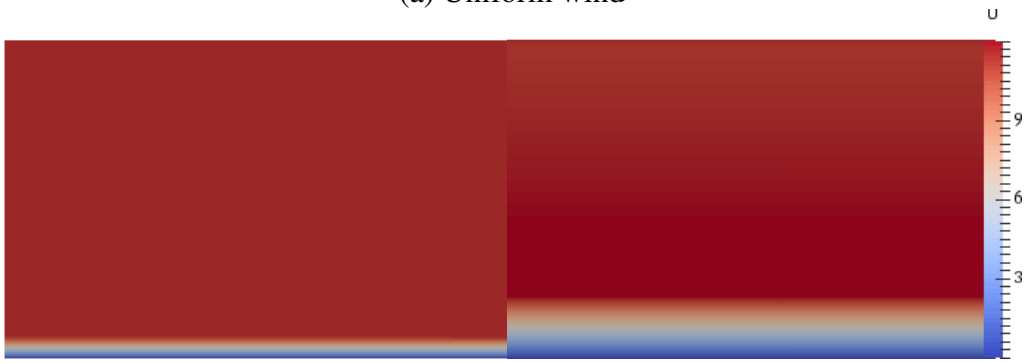

(b) Linear shear wind (c) Shear wind with wave-wind interaction

Figure 5. Initial wind speed for three cases

4. Results and Discussions

4.1 Aerodynamic Thrust and Torque

From the simulation, the time history of unsteady thrust and torque of the wind turbine are obtained. The time history of thrust and torque are shown in Fig6. Non-dimensional treatment is done on the thrust and torque results by dividing the thrust or torque by the mean value. And the time value t is divided by the rotating period of turbine rotor (T=4.96s).

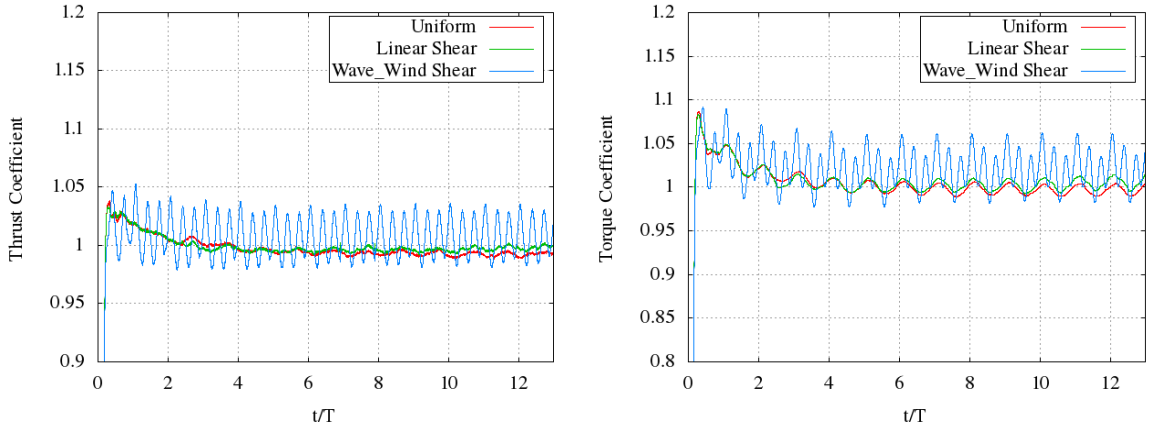

Figure 6.Aerodynamic thrust and torque

Both the aerodynamic thrust and torque show steady state after about 2~4 rotating periods. The aerodynamic thrust and torque coefficients in both case1 (uniform inflow wind) and case2 (linear shear wind distribution for 20m) shows slight oscillation with same period as turbine rotation, this is believed to be led by the shaft tilt of the rotor plane. The results in case1 and case2 are close, which can be explained with Fig.4 and Fig.5. As illuminated above, the wind speed distributions are the same in the turbine blades rotating areas (z>20m), so the aerodynamic forces are not quite different. Oscillation with much larger amplitude is observed on aerodynamic forces in cases3 (shear wind with wave-wind interaction). In case3, the wind speed is lower than 11.4m/s as height z<60m, while the wind speed grows larger than 11.4m/s in above areas, and turbine blades rotates at the range of 30<z<150. In this case, the aerodynamic forces on a blade rotates through the above area with higher wind speed will be larger than those aerodynamic forces on another blade in lower area with lower wind speed. As the three-blade wind turbine rotates periodically, the aerodynamic forces show periodic oscillating regularity with 1/3 of rotating period. Besides this oscillating regularity, it is also notable that the mean values of the aerodynamic forces in case3 are larger than those in the other two cases. With a close-up view of the curves in Fig.4, the velocity expanding in the height above z=57m is observed on the red line, which means the wind speed is over 11.4m at most of the turbine rotating areas. There's no doubt that the aerodynamic forces grows with the increasing wind speed.

4.2 Flow Field Description

The flow velocity distributions in longitudinal sections are shown in Fig.7. Compared with the initial wind speed shown in Fig.5, the flow velocity shows considerable reduction at the wake flow area as the green regions in the three figures. The upper regions (z>0) of the three figures have slight difference, because the wind speed in these regions are similar, especially for case1 and case2 of which the inflow wind speed are exactly the same in the above areas. Compare with case1, case2 and case3 show stronger interaction between the lower-speed region and the wake flow field of wind turbine. With this interaction, the flow velocity decreases around the lower border of wake flow in case 2 and case 3, in which cases the shape of the borderlines are changed, while the thickness of the lower-speed layer decreases, which means increase of flow velocity in the this lower-speed region.

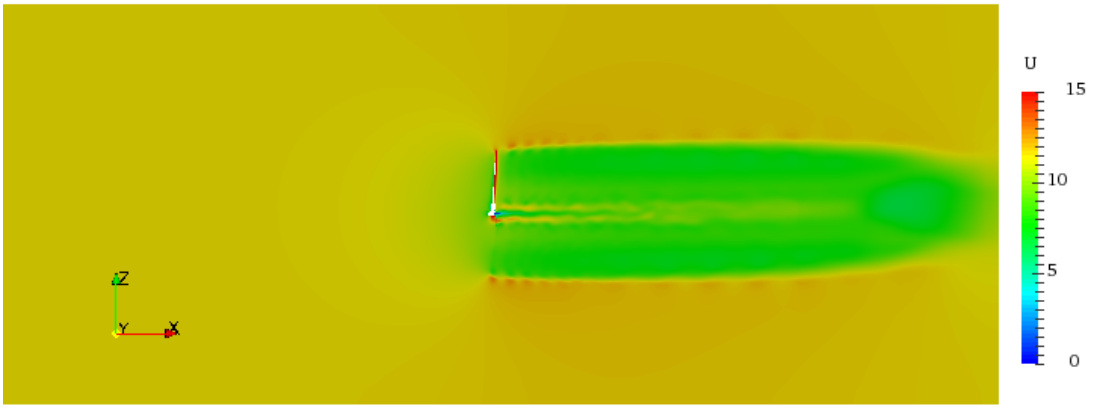

(a) case1: uniform inflow wind

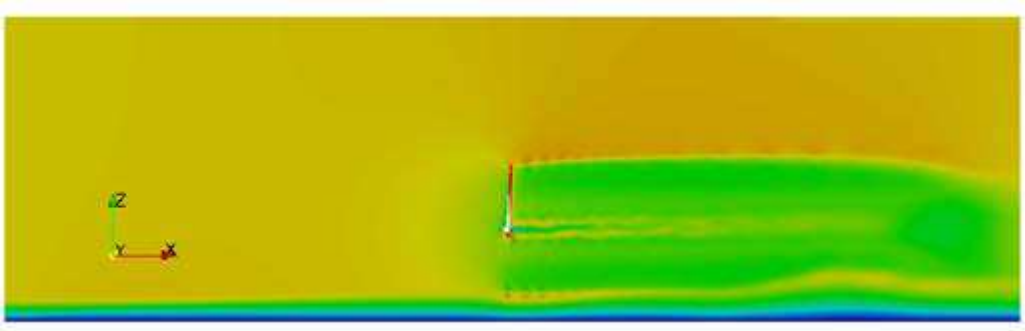

(b) case2: linear shear wind

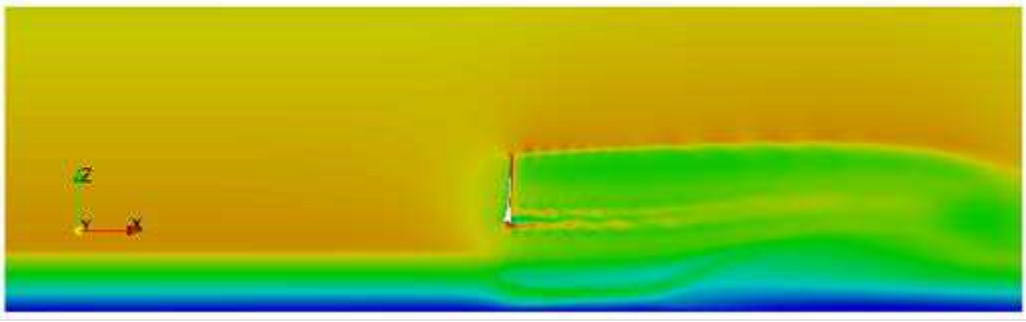

(c) case3: shear inflow wind with wave-wind interaction

Figure 7. Flow velocity distribution on longitudinal section

Fig.8 shows the flow velocity distribution on cross sections at six different locations along x direction. The location of the cross sections in order from upstream side to downstream region are: (a) x=-4m, (b) x=-1.2m, (c) x=2m, (d) x=5m, (e) x=15m, (f) x=50m, where the rotor center locates at x=0m. As the wind speed in the turbine rotation regions are the same in case1 and case2, the flow velocity distribution looks similar in (a)~(d), while differences appear in the last two sections.

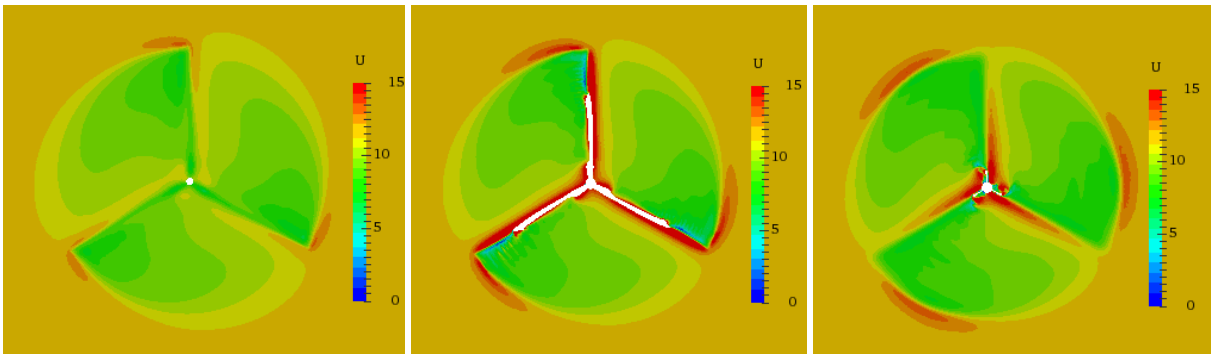

(a) x= -4m (b) x= -1.2m (c)x= 2m

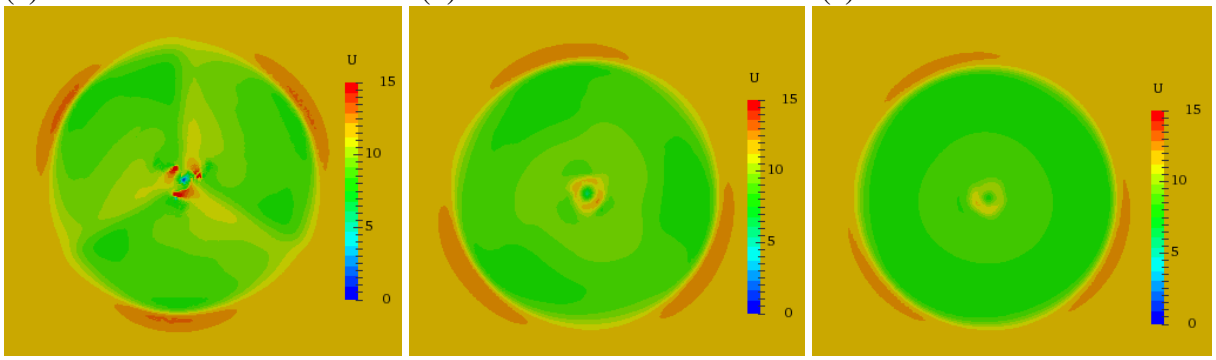

(d) x= 5m (e) x= 15m (f) x= 50m

Figure 8. Flow velocity distribution on cross sections in case1

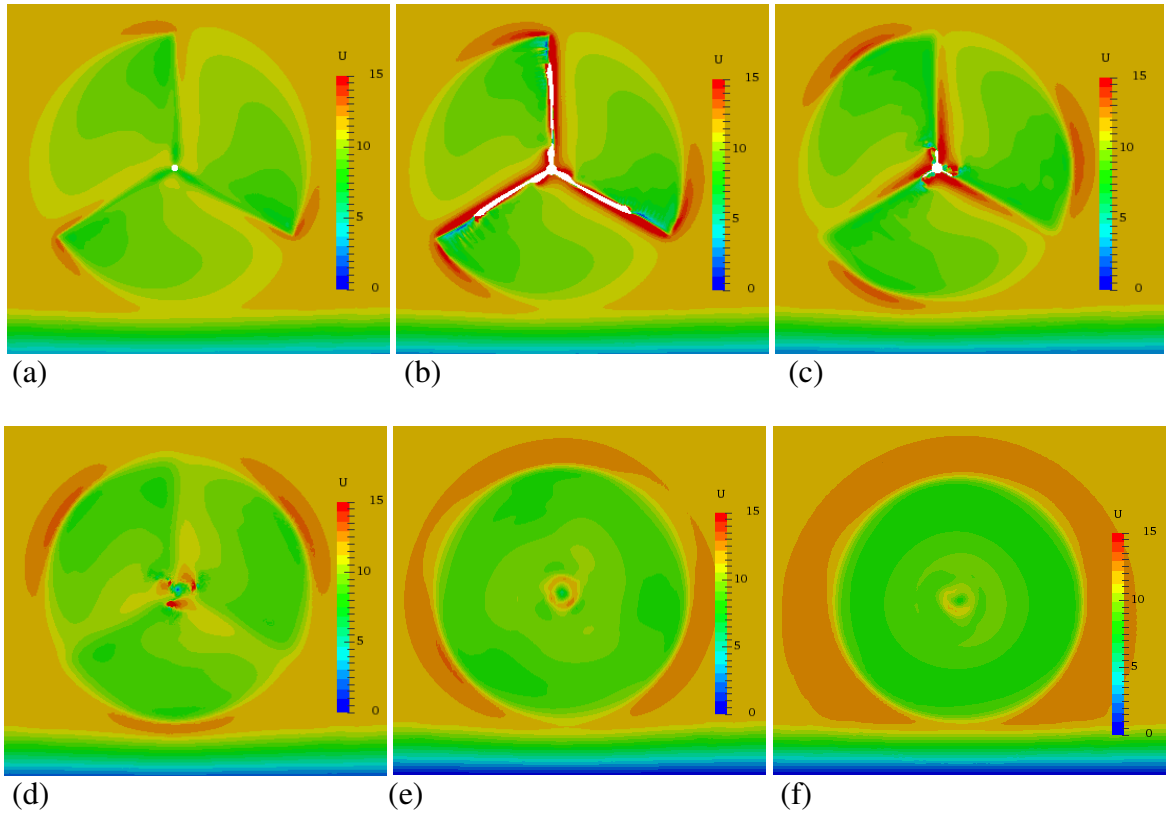

Figure 9. Flow velocity distribution on cross sections in case2

Disturbance of the rotating blade breaks the steady state of initial flow field near blades surface. With viscous effect, flow nearby the blade surface rotates with the blade, which then interacts with neighbor flow and the incoming flow with initial velocity, so the flow velocity in wake flow field decreases and wake vortex propagates to downstream field. In Figure8~11, the flow field are colored with flow velocity, where the red regions mean increased velocity, and green regions mean decrease of velocity. In each figure, red regions occur near the outer edge of wake vortex flow, which contains three pieces in most figures. These outer high-speed regions are the cross section of the spiral tip vortex (the wake vortex structures are shown in Fig.12). With interaction with neighbor flow, the flow velocity in wake vortex decreases slightly as the vortex propagates downstream. In case2 and case3, the flow velocity in spiral vortex near the lower-speed regions is reduced, while the vortex tubes become wider as shown in (d)~(f) in Fig.9~10.

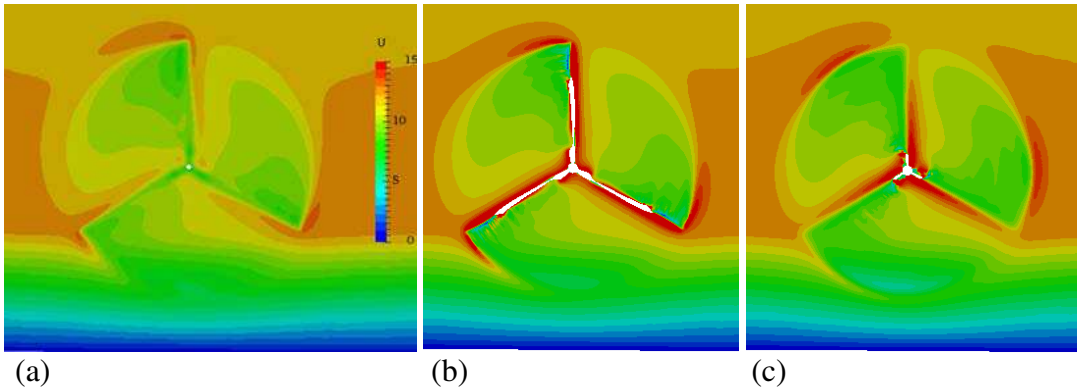

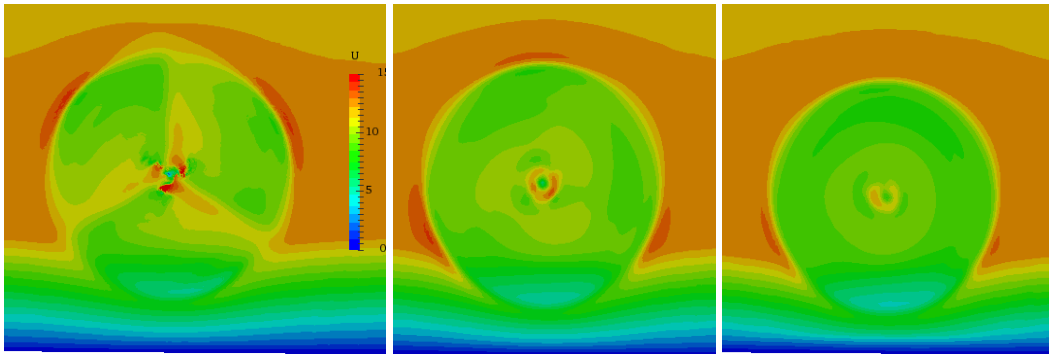

(d) (e) (f)

Figure 10. Flow velocity distribution on cross sections in case3

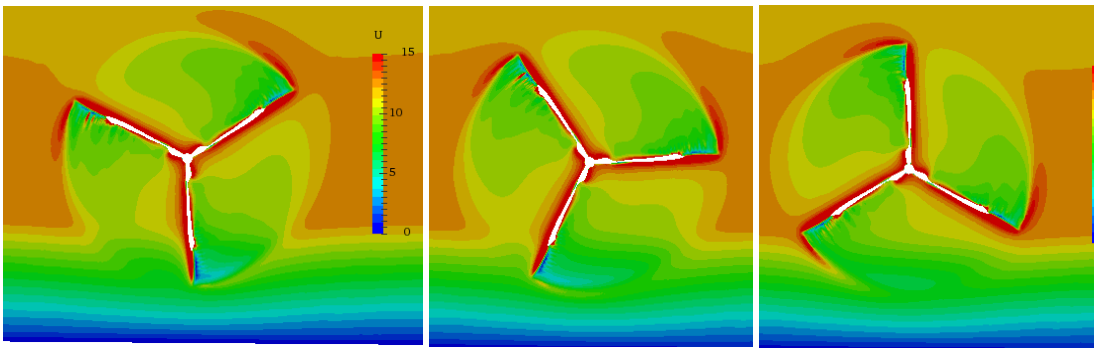

(a) t=50.8s (b) t=51.2s (c)t=51.6s

Figure 11. Flow velocity distribution on cross sections during 1/6 period

Flow velocity distributions nearby wind turbine at three typical moments are presented in Fig.11, which are selected as the moment when the aerodynamic forces reach the minimum, medium and maximum values. These three moments represents for different azimuth angles of the rotor: (a) t=50.8s, azimuth angle=3659deg, minimum value of aerodynamic forces (b) t=51.2s, azimuth angle= 3689deg, medium value of aerodynamic forces (c) t=51.6s, azimuth angle=3720deg, maximum value of aerodynamic forces. When the rotor rotates to the similar pose as (a), part of one blade submersed in lower-speed layer, which is bound to reduce the aerodynamic forces on this blade. As the three-blade wind turbine rotates at a fixed angular speed, this reduction occurs three times in every rotating period, just as shown in Fig.6.

4.3 Wake Vortex

Wake vortex structure is an important index in aerodynamic analysis, because the wake vortex near the blades affects the aerodynamic properties of the blades. To get a proper wake vortex visualization result, the second invariant of the velocity gradient tensor, Q (Digraskar D A, 2010), is used to capture the iso-surface of the vortex, which is:

$$Q = \frac{1}{2}(\|\Omega\|^2 - \|S\|^2) \tag{7}$$

Where S is the symmetric part of the velocity gradient tensor and Ω is the anti-symmetric part:

$$S_{ij} = \frac{1}{2}(\frac{\partial u_i}{\partial x_j} + \frac{\partial u_j}{\partial x_i}),\ \Omega_{ij} = \frac{1}{2}(\frac{\partial u_i}{\partial x_j} - \frac{\partial u_j}{\partial x_i}) \tag{8}$$

Fig.12 shows the visualization of wake vortex structures countered by value of Q=0.02. The wake vortex is mainly composed by three spiral tip vortex tubes and three root vortex tubes. The blade tip disturbs flow around its surface, and the rotating flow interacts with its neighbor flow, so the vortex start propagating downstream and the radius of the vortex tube increases

rapidly at beginning of vortex shedding. As discussed above, interaction with lower-speed layer induces the flow velocity in vortex, and makes the tube wider in case2 than that in case1, which accelerates the dissipation of wake vortex at the same time. As the lower-speed layer in case3 is much thicker, part of the blades is immersed in the lower-speed layer. The rotor blades rotates in the same fixed angular speed as in case1 and case2, so the disturbances to wind flow are similar, but the interaction with the lower-speed flow makes the flow velocity decreased significantly in lower-speed layer, as shown in Fig.12(c). The x-component of flow velocity, which mainly comes from the inflow velocity, is the key factor that makes the wake vortex propagating downstream. So the distance between two neighbor vortex tubes narrows down distinctly.

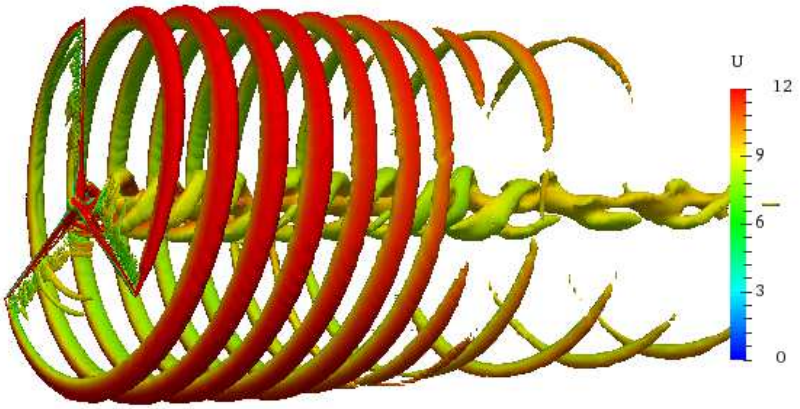

(a) case1: uniform inflow wind

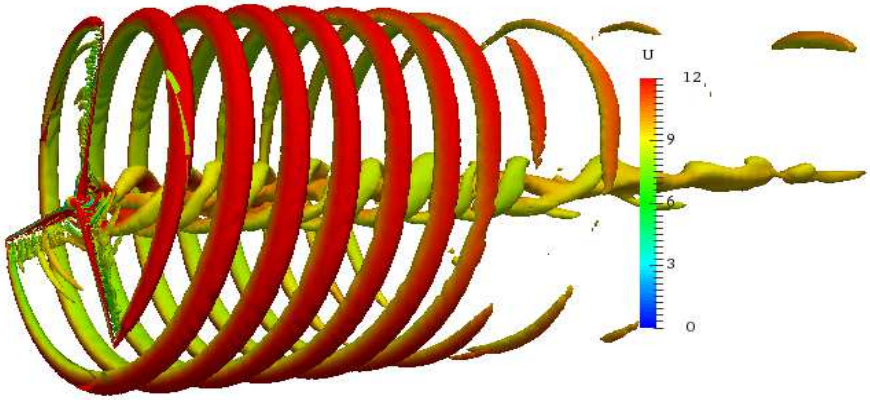

(b) case2: linear shear inflow wind

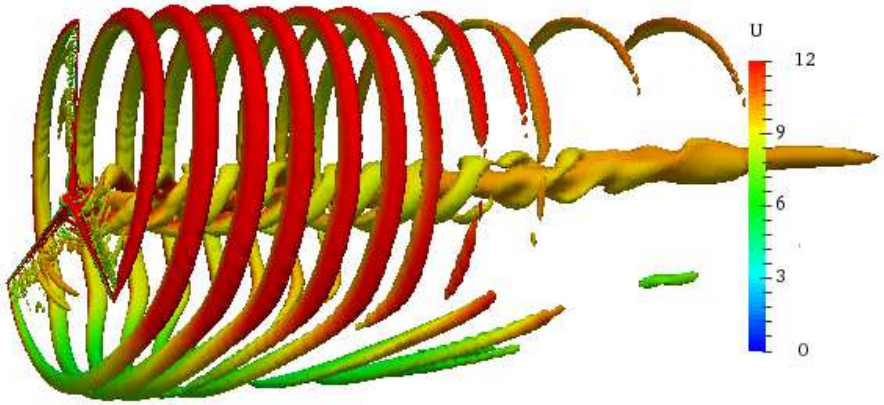

(c) case3:shear wind with wave-wind interaction

Fig.12 visualization of wake vortex structures

Conclusions

In this paper, the interaction between wave and wind is studied first to get a proper shear wind model for unsteady aerodynamic simulations with non-uniform inflow wind. The wind speed is reduced when passing through the wave surface. The wave surface elevation has slight influence on the flow velocity distribution above certain height (z>30m), so a fitted curve is obtained and employed as distribution of inflow velocity on inlet boundary.

Aerodynamic simulations in three different inflow wind conditions are conducted. Compared with the uniform inflow case, the linear shear wind with lower-speed layer totally below the blades rotating region has negligible effect on the aerodynamic forces of the wind turbine, while the interaction phenomenon between its wake vortex and the neighbor flow is observed. This interaction effect is much pronounced when the lower-speed layer overlaps the rotating region of turbine blades. The aerodynamic forces on the part of blades which is immersed in lower-speed layer are reduced, so the aerodynamic forces of the whole rotor oscillates with 1/3 rotating period.

Acknowledgements

This work is supported by the National Natural Science Foundation of China (51379125, 51490675, 11432009, 51579145), Chang Jiang Scholars Program (T2014099), Shanghai Excellent Academic Leaders Program (17XD1402300), Program for Professor of Special Appointment (Eastern Scholar) at Shanghai Institutions of Higher Learning (2013022), Innovative Special Project of Numerical Tank of Ministry of Industry and Information Technology of China (2016-23/09) and Lloyd's Register Foundation for doctoral student, to which the authors are most grateful.

References

Atcheson M. (2016). Floating Offshore Wind Energy.

Bayne S B, Giesselmann M G. (2000). Effect of blade passing on a wind turbine output[C]. Energy Conversion Engineering Conference and Exhibit, 2000.(IECEC) 35th Intersociety. IEEE, 2: 775-781.

Bazilevs Y, Hsu M C, Akkerman I (2011). 3D simulation of wind turbine rotors at full scale. Part I: Geometry modeling and aerodynamics [J]. International Journal for Numerical Methods in Fluids, 2011, 65(1- 3): 207-235.

Carrica P M, Huang J, Noack R (2010) Large-scale DES computations of the forward speed diffraction and pitch and heave problems for a surface combatant [J]. Computers & Fluids, 39(7): 1095-1111.

Digraskar DA (2010). Simulations of flow over wind turbines [J]. Diffraction and pitch and heave problems for a surface combatant. Comput. Fluids 39 (7), 1095–1111.

Dolan D S L, Lehn P W. (2006). Simulation model of wind turbine 3p torque oscillations due to wind shear and tower shadow [J]. IEEE Transactions on energy conversion, 21(3): 717-724.

Jonkman, J, Butterfield, S, Musial, W, Scott, G (2009). Definition of a 5-MW reference wind turbine for offshore system development. Golden, CO: National Renewable Energy Laboratory.

Lindenburg C (2002). Aeroelastic modelling of the LMH64-5 blade [J]. Energy Research Center of the Netherlands, Technical Report No. DOWEC-02-KL-083/0, DOWEC 10083_001.

Menter FR(1994). Two-equation eddy-viscosity turbulence models for engineering applications [J]. AIAA journal, 32(8): 1598-1605.

Noack, RW (2005). SUGGAR: a general capability for moving body overset grid assembly. In: Proceedings of the 17th AIAA Computational Fluid Dynamics Conference, American Institute of Aeronautics and Astronautics, Toronto, Ontario, Canada.

Thiringer T, Dahlberg J A. (2001). Periodic pulsations from a three-bladed wind turbine[J]. IEEE Transactions on Energy Conversion, 16(2): 128-133.